Phasor and EMT Models of Grid-Following and Grid-Forming Converters for Short-Circuit Simulations

Vinicius Albernaz Lacerda, Eduardo Prieto Araujo, Marc Chea-Mañe, Oriol Gomis-Bellmunt

***Abstract*—Phasor models have been widely used in short-circuit simulations, in which system operators verify the behaviour of the grid over thousands of different contingencies. However, it is still unclear if phasor models can still be used in fault studies in modern or future power grids dominated by renewable generation with power electronics and converters. Therefore, this paper analyses the suitability of phasor models to simulate short-circuit transients in grids with grid-following (GFL) and grid-forming (GFM) voltage-source converters (VSC). Phasor models of GFL and GFM were developed and tested in two test systems, one with 50% of converters in the generation mix and another powered 100% by converters. Asymmetrical and symmetrical faults were applied at different points of the systems and key variables were used to compare the phasor models against EMT models during the transients. The results showed that, despite neglecting transients in the grid, phasor models could be used in a preliminary stage of short-circuit studies as it was capable of tracking the steady-state value of almost all variables analysed. In this case, detailed EMT simulations, although necessary, would be used only at more advanced stages of the studies.**

***Keywords*—grid-following VSC, grid-forming VSC, phasor model, short-circuit transients.**

I. Introduction

SHORT-CIRCUIT studies are part of numerous simulations performed by transmission system operators when analysing power grids. In the past, when power systems were composed mainly of rotating machines such as synchronous generators (SGs), the boundary between electromagnetic transients and electromechanical transients was very well established and phasor models were largely used to simplify and speed up simulations [1]. However, with the large integration of renewable generation and extensive use of power electronics, power system dynamic behaviour is becoming progressively faster, requiring previous assumptions to be revisited [2]. In this context, it is often unclear if phasor models are still suitable for simulating faults in modern power grids or if detailed Electromagnetic Transient (EMT) models are necessary in all cases.

The inclusion of new power converters in the grid with different electrical and control structures such as grid-following (GFL) and grid-forming (GFM) Voltage-Source Converters (VSC) are fostering the proposal of new simulation methods. One example is the co-simulation [3]–[5], where the grid is often modelled in phasor or another low-frequency equivalent model while the converter or power electronics device is modelled in EMT. However, as modern power grids have a high penetration of converters and power electronics, the area of the grid modelled in EMT starts to become as large as the area modelled in phasor, reducing the benefits in terms of simulation speed. Other modelling approaches aim to model more accurately the fast dynamics of power electronics but keeping the computational cost lower than in EMT. Some exampless are Dynamic Phasors [6]–[8], Harmonic State-Space modelling [9]–[11], Harmonic Phasor Domain [12] and frequency-dependent equivalents [13]. Although these methods are promising, phasor and EMT are still the main options for industry and system operators to analyse short-circuit scenarios. Moreover, although important recommendations and guidelines were recently available [14]–[16], indicating that EMT models are imperative for such converters, the suitability of phasor models for simulating short-circuits in 100% converter-based grids still needs further investigation.

Therefore, this paper presents GFL and GFM phasor models that can be used to simulate renewable sources based on VSC converters. It analyses the suitability of these phasor models to simulate symmetrical and asymmetrical faults with GFL and GFM converters.

The paper is organized as follows. Section II introduces average EMT models for GFL and GFM. Section III introduces VSC phasor models for GFL and GFM VSC. Section IV presents the methodology to conduct the comparative analysis. The results are shown in Section V along with discussions. Finally, the conclusions are drawn in Section VI.

II. VSC EMT Models

When performing short-circuit simulations, it is often not important to consider the harmonic content generated by the converter's switching. In this case, it is useful to use the converter average (AVG) model. The EMT AVG model

This work was supported by the European Union's Horizon 2020 Research and Innovation Program [Powering System Flexibility in the Future through Renewable Energy Sources (POSYTYF) Project] under Grant 883985. The work of Oriol Gomis-Bellmunt was supported by the Institució Catalana de Recerca i Estudis Avançats (ICREA) Academia Program V. A. Lacerda, E. Prieto, M. Chea and O. Gomis are with Centre d'Innovacio Tecnològica en Convertidors Estatics i Accionaments, Universitat Politècnica de Catalunya (CITCEA-UPC), 08034 Barcelona, Spain (e-mails: vinicius.lacerda@upc.edu, eduardo.prieto-araujo@upc.edu, marc.cheah@upc.edu and oriol.gomis@upc.edu).

Paper submitted to the International Conference on Power Systems Transients (IPST2023) in Thessaloniki, Greece, June 12-15, 2023.

neglects the converter's switching and considers that the VSC output voltage is an amplified form of the modulation index defined by the control [17]. Thus, the VSC electrical model on the AC side is simply a controlled voltage source whose inputs are the inner loop (current control) voltage references. In the AVG model, the converter DC-side is electrically decoupled from the AC side and its dynamics can be represented using the power exchanged with the grid. However, in this study, an ideal DC-side was considered and such dynamics were neglected.

A. Grid-following (GFL)

The GFL VSC controls the current that is injected into the grid. To achieve this behaviour it measures the grid voltage (v_g) and applies an internal voltage (v_c) such that the current defined by the control loops (i_c) is achieved, as shown in Fig. 1. Therefore, the GFL acts as a current source. The abc voltages and currents are transformed to dq frame using the Park transform, indicated as $T(\theta)$ in Fig. 1. The synchronized θ used in the Park transform is obtained from the Phase-locked Loop (PLL) aligned with v_q such that $v_d = 0$. In this study, the conventional synchronous reference frame PLL (SRF-PLL) and tuning described in [18] was used.

The GFL control was modelled using a well-known structure composed of an inner loop and an outer loop. The inner loop controls the output current (both positive and negative sequence) in the qd frame using the double synchronous reference frame (DSRF) [19]. The outer loop controls active and reactive powers. PI controllers are used in both loops. In this study the inner-loop PI controller gains were tuned using the internal model control approach [20] while the outer-loop PI controllers were tuned according to the modulus optimum criteria [21]. The current limit (I_{max} in Fig. 1) was set to 1.2 p.u.

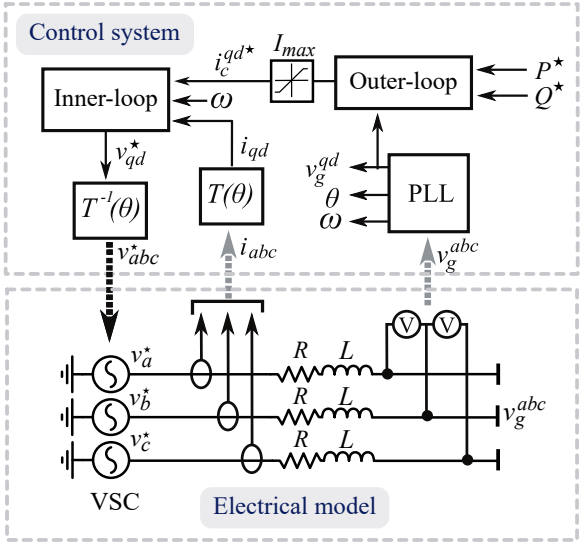

Fig. 1. GFL VSC EMT average model.

As the DSRF allows controlling both positive and negative sequence currents, a sequence extraction technique is required. In this study, the Delayed Signal Cancellation (DSC) method [22] was used. The PLL was aligned with the positive sequence voltage (v_g^{q+}). The positive sequence currents i_c^{dq} were defined by the outer loop but the negative sequence currents could be controlled with different objectives. Thus, the defined setpoint was to inject zero negative sequence currents $i_c^{q-\star} = 0$ and $i_c^{d-\star} = 0$.

B. Grid-forming (GFM)

The main difference between the GFM VSC and the GFL is that the GFM acts as a voltage source, imposing its own angle and voltage magnitude, without the need for a PLL. Therefore, the GFM does not need an external grid to operate. Several control schemes were proposed for GFMs, such as droop-based control [23], [24], virtual oscillator control [25], matching control [26], virtual synchronous machine control [27], [28], among others [29], [30]. In this study, the cascaded voltage control and droop synchronization method was used, similar to the one used in [31]. In this scheme, the VSC controls the voltage v_s of its filter capacitor (Fig. 2) and the frequency is defined by the active power droop. In Fig. 2 LPF means low-pass filter, ω_n and V_n are the nominal frequency and voltage, respectively.

The DSRF was also used in the GFM, allowing controlling both positive and negative sequence voltages. The positive sequence voltage (v_s^{q+}) was defined to be 1 p.u and the negative sequence voltage references were defined as zero $v_s^{q-\star} = 0$ and $v_s^{d-\star} = 0$. By doing this, the GFM was able to compensate unbalances in the grid voltages. Although this is not aligned with actual standards and grid codes, this strategy was chosen for the purpose of promoting further research in the best practices related to fault-ride through, as also performed by other works [32].

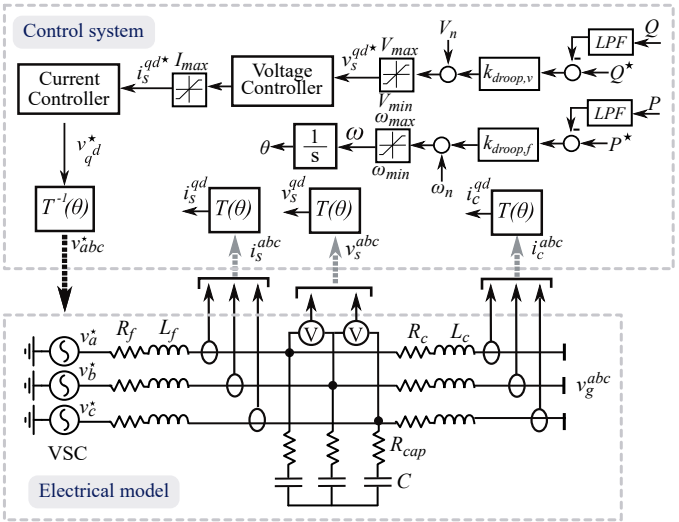

Fig. 2. GFM VSC EMT average model.

The virtual inertia (active power filter time constant) was chosen as 20 ms, allowing fast synchronization between multiple converters.

The limits for positive ($I_{max,pos}$) and negative ($I_{max,neg}$) sequence currents were defined dynamically, respecting a maximum current I_{max} of 1.15 pu. In this strategy, static limits are defined for one sequence (positive or negative),

and the remaining capacity is dynamically defined for the other sequence, such that their sum never exceeds I_{max} [33]. Different prioritizations can be chosen, such as voltage magnitude prioritization (injection of positive sequence currents) or voltage balance prioritization (injection of negative sequence currents) [34]. In this paper voltage balance prioritization was used. Thus, the priority was to inject reactive negative sequence current i_{d-} during the fault.

III. VSC Phasor models

In phasor simulation, the grid differential equations defining the system electromagnetic transients are substituted by algebraic equations of the form $\mathbf{V} = \mathbf{ZI}$, where $\mathbf{V}$ and $\mathbf{I}$ are the complex-valued vectors of node voltages and current injections, and $\mathbf{Z}$ is the impedance matrix.

Because of this simplification, larger simulation time steps can be used and the simulation speed can be greatly increased. This is especially interesting when simulating several cases in large networks. However, as electromagnetic transients are neglected in phasor models, their suitability needs to be carefully evaluated as the simulations can provide overestimated or underestimated values.

As phasor simulation is used mainly to simplify simulations, several approximations can be performed in the VSC control system to allow using larger simulation time steps. In this study, the VSCs were represented as current sources with magnitude and angle defined by the control system and the VSC inner control was completely removed. Therefore, the outer loop needs to be readjusted to keep the total control closed-loop time constant equal to the original closed-loop time constant, as shown in [35].

As in phasor simulation the voltage measurements are complex numbers, the phase is readily available and no PLL is needed when simulating GFL. Hence, to have $v_d^+ = 0$ as in EMT, is only necessary to take the angle (θ) of the grid positive sequence voltage and rotate the voltages and currents in the abc frame with respect to this angle. Then, after the rotation, the q axis becomes the real part of the complex variable and the d axis the imaginary part, or vice versa depending on the convention used. Positive and negative sequences are calculated using Fortescue's theorem. This also neglects the dynamics related to the sequence extraction in EMT, performed by filtering or by DSC. The phasor model of the GFL VSC is shown in Fig. 3.

To develop the phasor model of the GFM, a similar approach as the one used in GFL The same approach was used for developing the phasor model of the GFM. The current controller was neglected and the current reference ($i_s^{qd\star}$) defined by the voltage controller was directly transformed to the abc frame and sent to current sources. Other phasor models are also possible, considering for example the current controller as a first-order transfer function or even the whole loop with its PI controllers. The more detailed the control is, the smaller the time step required to simulate the model.

Differently from the GFL, the GFM does not align with the grid angle by measuring it from a PLL but defines its own angle. Therefore, the angle (θ) used in the rotation to the qd frame is calculated as the integral of the difference between frequency ω defined by the synchronization loop and the base frequency of the phasor simulation (50 Hz in this case). The phasor model of the GFM VSC is shown in Fig. 4.

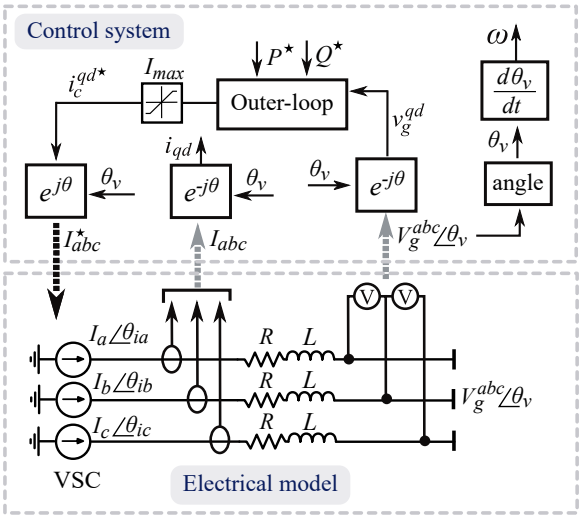

Fig. 3. GFL VSC phasor model.

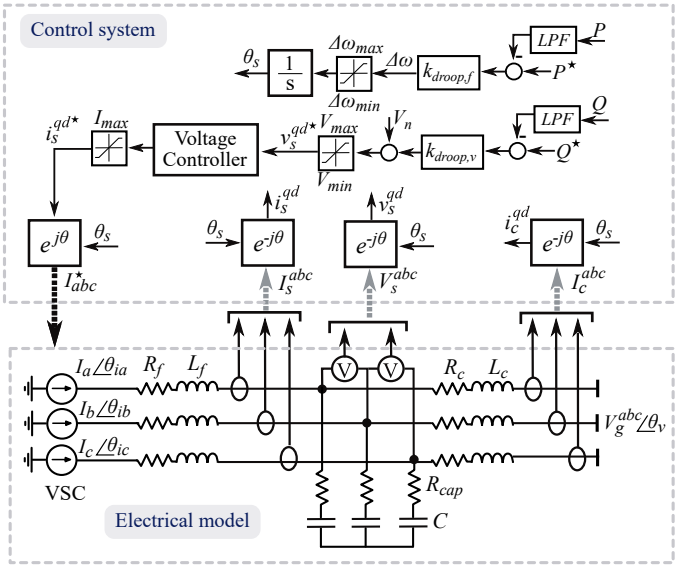

Fig. 4. GFM VSC phasor model.

IV. Methodology

To assess the suitability of phasor models of GFL and GFM VSCs for short-circuit simulations, different fault cases were performed in two test systems. The first system is shown in Fig. 5. It was composed of both SGs and GFL converters, with a share of 50% in the generation. The second system is shown in Fig. 6. It was composed only of converters, with a share of 50% GFM and 50% GFL. The transmission system was a modified version of scenario 3 in [36]. Both systems were simulated in Simulink using a fixed-time step (10 μs in EMT and 100 μs in phasor) and the Euler solver (algorithm *ode1* in Matlab). The system parameters are summarized in

the Appendix. In the tests, the GFM reactive droop was not activated, thus $v_q^\star = V_n$ and $v_d^\star = 0$.

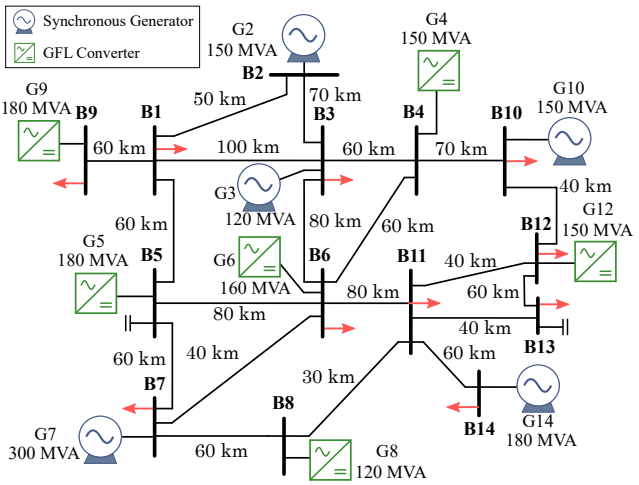

Fig. 5. Test system 1 - grid with SGs and converters.

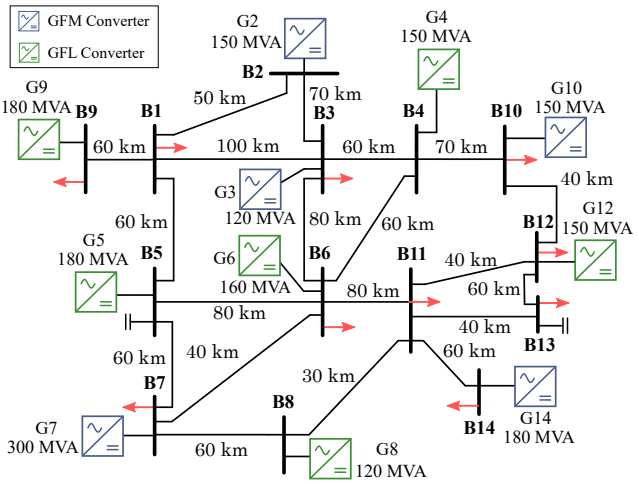

Fig. 6. Test system 2 - 100% converter-based grid.

The simulated cases were:

1) Case 1: 10 Ω AG fault at B10 of test system 1.

2) Case 2: 1 Ω three-phase fault at B1 of test system 1.

3) Case 3: 10 Ω AG fault at B10 of test system 2.

4) Case 4: 1 Ω three-phase fault at B1 of test system 2.

The duration of all fault cases was 200 ms. These cases represent symmetrical and asymmetrical faults at different locations of the system.

V. Results

The results for each test case are discussed in this section. Due to the large amount of variables generated in the simulations, a selection of key variables of the converters closer to the faults were shown. The variables of GFL converters are discussed in the first test system and the variables of GFM converters are discussed in the second test system.

A. Test system 1 - Grid with SGs and converters

1) Case 1: single-phase fault at B10. The results for this case are shown in Fig. 7. As can be observed in Fig. 7, the phasor models could track the abc and dq voltages and currents with a good accuracy despite minor deviations. However, as the phasor model neglects electrical dynamics and does not include PLL, fast transients associated with the fault are not represented in this model. As an example, the oscillatory behaviour of the negative sequence controllers (Fig. 7e and Fig. 7f) due to the non-ideal performance of positive and negative sequence separation are neglected in phasor, because extracting the sequence components in phasor is directly done using Fortescue's theorem.

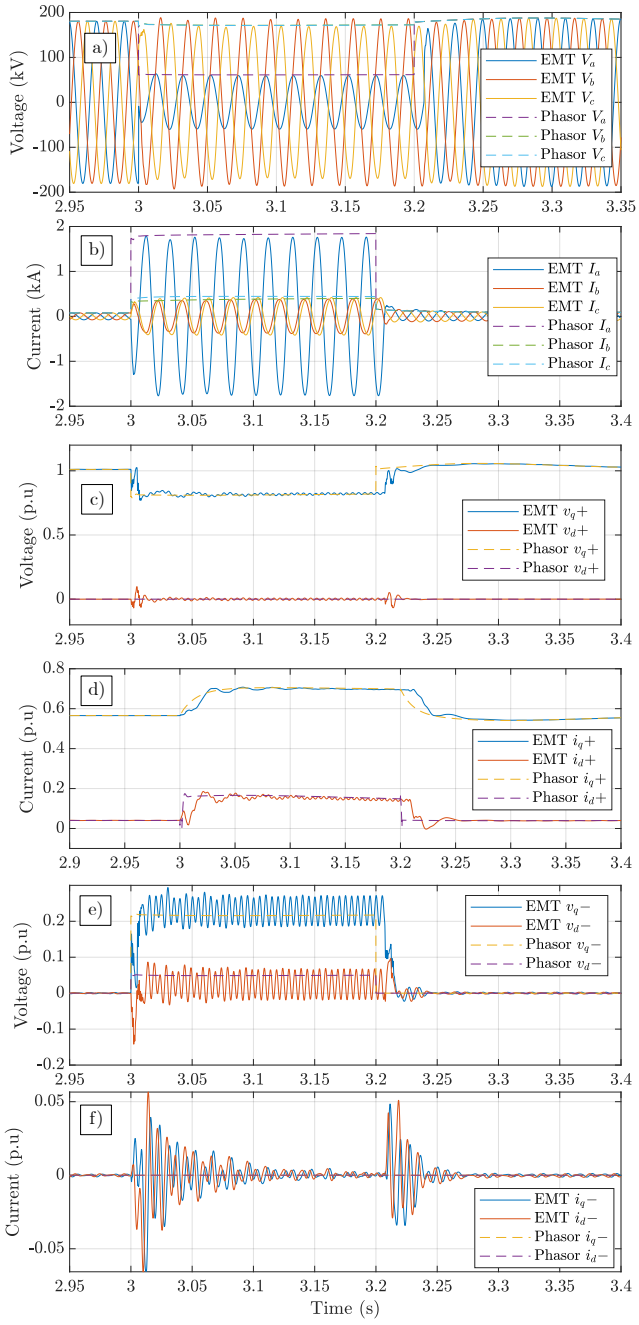

Fig. 7. Case 1 a) B10 voltage b) B10 current c) G4 v_g^{qd} positive sequence d) G4 i_c^{qd} positive sequence e) G4 v_g^{qd} negative sequence f) G4 i_c^{qd} negative sequence.

2) Case 2: three-phase fault at B1. The results for this case are shown in Fig. 8. As can be observed in Fig. 8, the fault dramatically reduced the voltage. This voltage drop negatively

influenced the GFL converter's PLLs. As a simple PLL was used in this cases, when the voltage dropped to a very low level the PLL could no track the grid voltage angle correctly. As this angle is used to calculate both positive and negative sequence currents and voltages in the dq frame, the converter was not able to correctly control the negative sequence currents to zero (although the fault was symmetrical), as shown in Fig. 8e and Fig. 8f. Moreover, due to the loss of synchronism, the output current exceeded the maximum value despite the current references being limited to I_{max}. Due to this wrong operation of the PLL, the differences between phasor and EMT were more pronounced in this case. Moreover, as in phasor the angle is obtained by the $arctan$ of the division between the imaginary and real part of the voltage, when the voltage was low, the oscillations in the rest of the system affected the division more and subsequently the angle used in the dq components, as can be seen in Fig. 8c and Fig. 8d. Despite these deviations, the phasor was able to track the abc voltages and currents after the initial transient, as can be observed in Fig. 8a and Fig. 8b.

B. 100% converter-based grid

In the second test system all SGs were substituted by GFM converters with fast control, low virtual inertia and limited overloading capability. The power flow was kept the same when substituting the SG by GFM converters. Also, the GFM converters were programmed to reduce negative sequence voltages during the fault by injecting negative sequence currents. The objective was not to follow a specific grid code, but to verify if the phasor models can track the negative sequence current injection performed in EMT.

1) Case 3: single-phase fault at B10. The results for this case are shown in Fig. 9. The phasor model was able to track the grid voltages and currents, as can be observed in Fig. 9a and Fig. 9b. However, more pronounced deviations could be observed in the GFM converter internal voltages and currents in the dq frame, both during and after the fault (Fig. 9c and Fig. 9d). Although the converter was injecting reactive negative sequence current (i_{d-}) to reduce the negative sequence voltage, the required current to totally compensate for the voltage unbalance was higher than the converter limits. Thus, because of this limitation in the current, the internal voltage unbalance was mitigated, but not eliminated, as can be observed in Fig. 9e and Fig. 9f. Fig. 9e and Fig. 9f also show that the phasor model of the GFM could fairly track the magnitude of the three-phase voltages and currents even during an asymmetrical fault. This feature cannot be observed in phasor models based on positive sequence only, commonly used in commercial tools. This highlights the need to include also negative sequence modelling in such platforms.

2) Case 4: three-phase fault at B1. The results for this case are shown in Fig. 10. For this case, the phasor model tracked correctly all variables during the fault, although presenting larger deviations after the fault is removed. At the beginning of the fault, the converter injects a higher current due to the combined effect of the energy stored in the filter capacitor and the controller objective to keep its voltage close to the nominal value (Fig. 10c and Fig. 10f). The phasor model

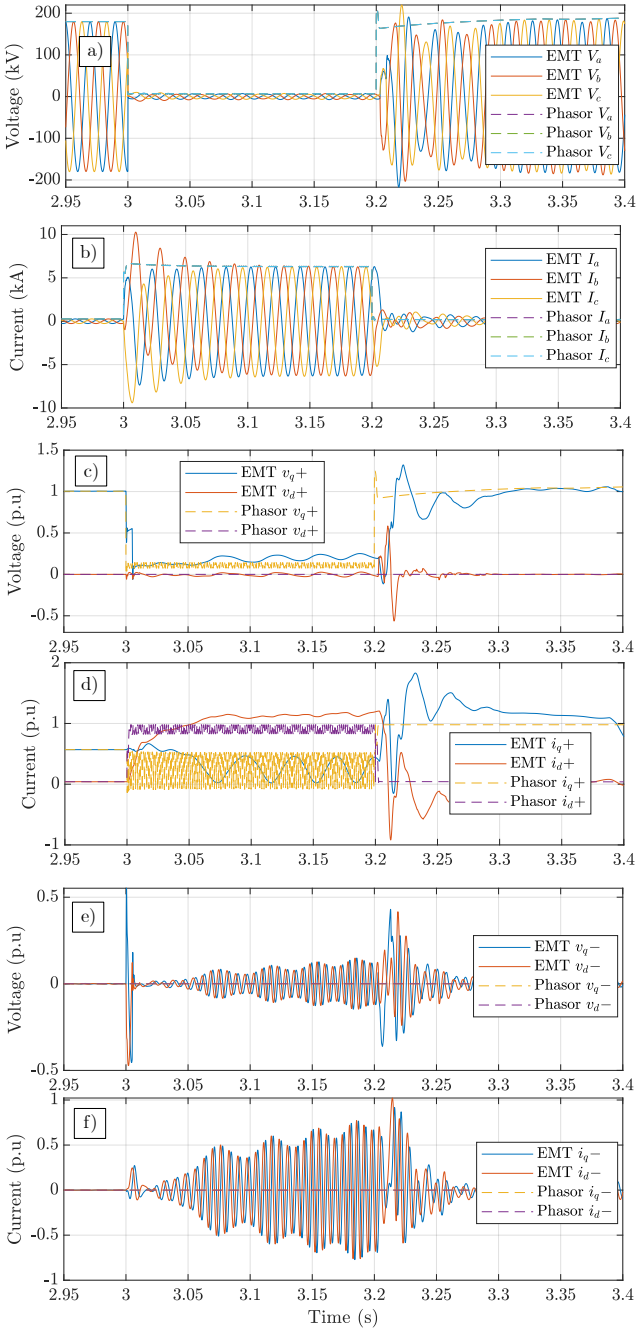

Fig. 8. Case 2 a) B1 voltage b) B1 current c) G9 v_g^{qd} positive sequence d) G9 i_c^{qd} positive sequence e) G9 v_g^{qd} negative sequence f) G9 i_c^{qd} negative sequence.

was able to track the control but did not represent the initial transient spike given by the capacitor discharge. It did not also show the transient in the negative sequence currents. After the fault is removed, a large transient occurred in the grid as the converters were synchronizing again. This effect was not correctly tracked by the phasor model. These results highlight the contribution of the converter filter in its transient response. Such electrical transients are not related to the control strategy, are not considered in the phasor model and can play an important role in the analysis depending on the type of study being performed.

In general, the major causes of difference between the EMT

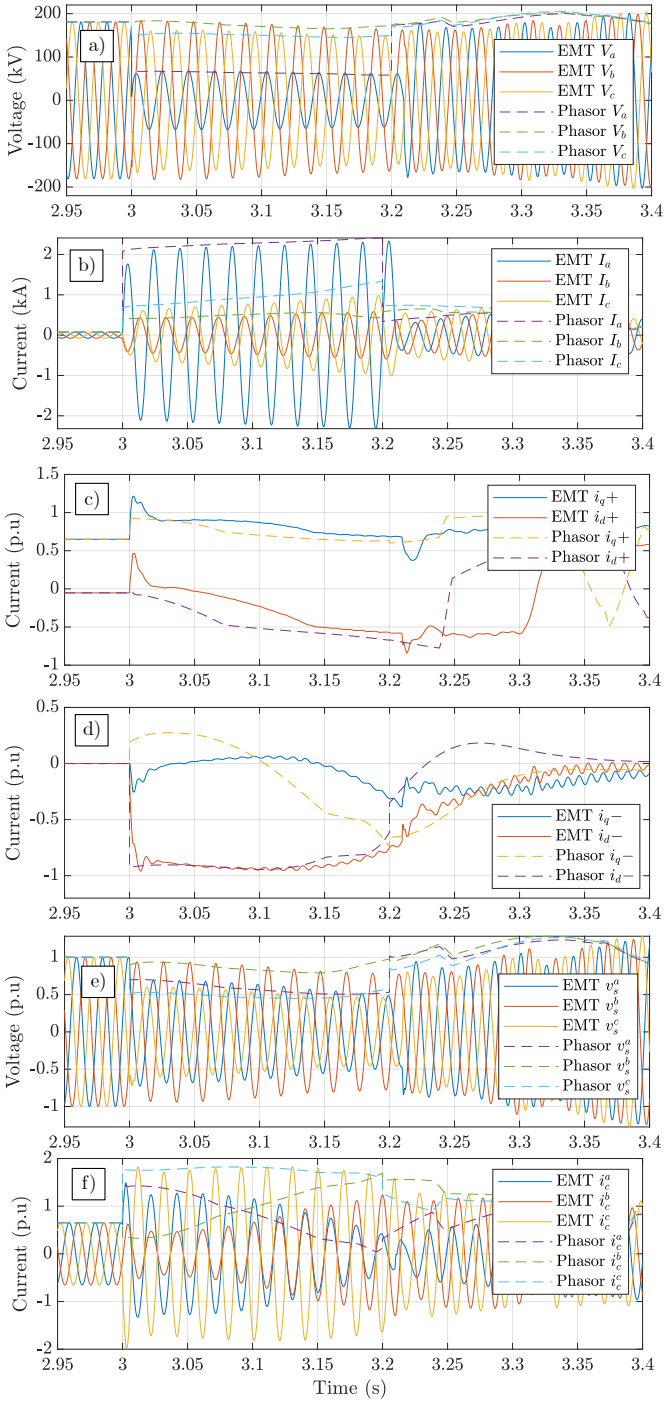

Fig. 9. Case 3 a) B10 voltage b) B10 current c) G10 i_c^{qd} positive sequence d) G10 i_c^{qd} negative sequence e) G10 v_s^{abc} f) G10 i_c^{abc}.

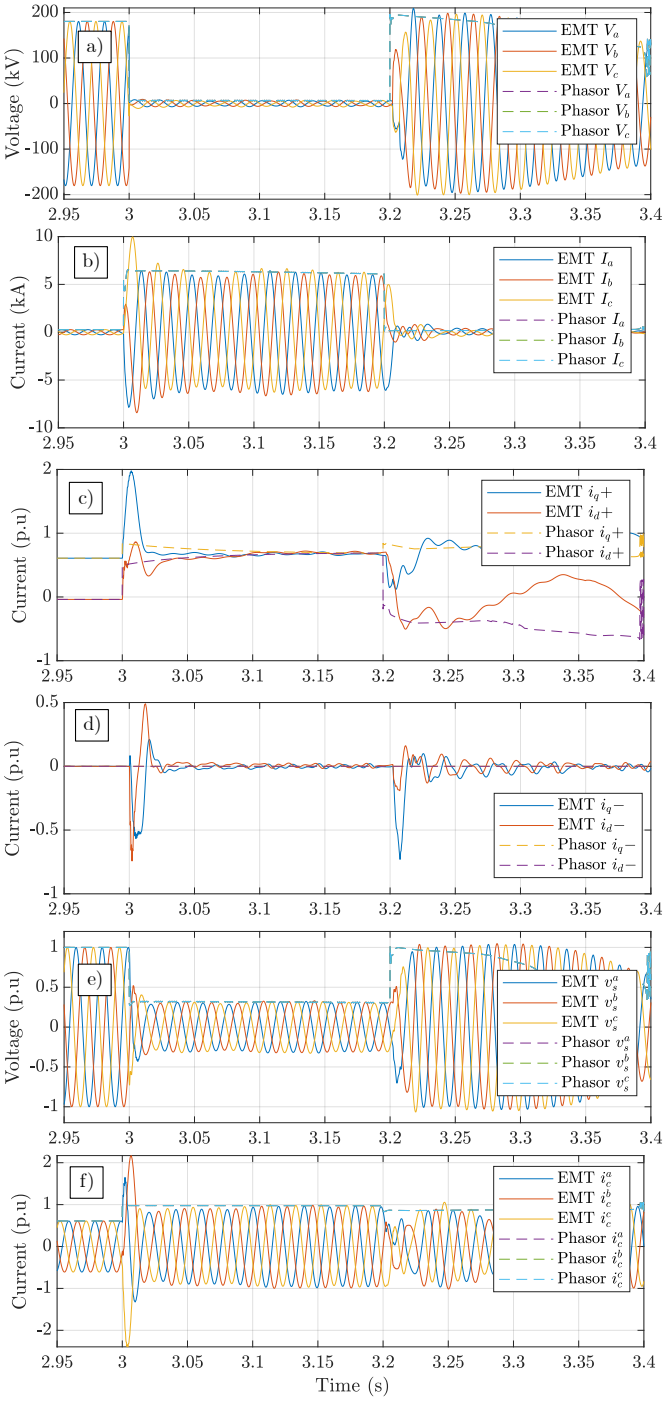

Fig. 10. Case 4 a) B1 voltage b) B1 current c) G2 i_c^{qd} positive sequence d) G2 i_c^{qd} negative sequence e) G2 v_s^{abc} f) G2 i_c^{abc}.

and phasor models of GFL and GFM converters in this study were the PLL, the sequence (positive and negative) calculation technique and the filter transients.

VI. Conclusions

This paper analysed EMT and phasor models of GFL and GFM converters currently used to simulate renewable sources in grid integration studies. The suitability of phasor models for simulating short-circuit transients in modern power grids was analysed based on a comparative study against EMT models. We addressed a gap related to the suitability of phasor models for short-circuit studies in modern power grids, with a high penetration of converters or even fully powered by converter-interfaced generation. In such scenarios, the boundary between electromagnetic transients and electromechanical transients overlap and a careful analysis is required before using phasor models.

From the tests performed it could be observed that, depending on the variables being observed in the simulation, the phasor models can still be used in several scenarios. Although the PLL and its interactions with the grid transients are not represented in phasor models, almost all variables

could be tracked with minor errors after the initial transient in the first test system. However, for extreme cases of large transients and deep voltage sags, the phasor model presented higher deviations. Also, as the phasor models do not model the PLL, it can be too optimistic in cases where the PLL loses synchronism with the grid, which is correctly captured in EMT simulations. When the grid was fully powered by converters, the dynamics were faster and the phasor model deviated more from the EMT. However, despite losing fast transients and high-frequency converter interactions, phasor models could still be used in preliminary studies involving large grids, as they model the average behaviour of the converters with reasonable accuracy. The suitability of phasor models for simulating specific phenomena such as sub-synchronous resonance or very weak grids need to be analysed more in-depth in future studies.

As the interest of industry and transmission system operators increases in simulating modern power grids with GFL and GFM converters, the analysis provided contribute to the discussion about suitable models of converters. As numerous short-circuit simulations are typically required, the use of phasor models allows simulating power grids much faster than in EMT. Thus they are useful at preliminary stages of the studies. In more advanced stages, detailed EMT simulations of selected cases are still required to analyse transients and higher frequency dynamics precisely.

VII. Appendix

The parameters of SGs, GFL and GFM converters were summarized in Tables I, II and III, respectively. The transmission lines were all 220 kV with the following parameters at 50 Hz: $R_1 = 0.0686\,\Omega$/km, $R_0 = 0.3936\,\Omega$/km, $L_1 = 1.28$mH/km, $L_0 = 3.68$mH/km, $C_1 = 9.16$ nF/km and $C_0 = 6.58$ nF/km.

TABLE I
Synchronous generators parameters.

Parameter	$G2, G10$	$G7$	$G3, G14$
V_n (kV)	22.0	22.0	22.0
X_d (pu)	2.20	1.25	1.667
X_q (pu)	2.00	1.00	1.125
X'_d (pu)	0.30	0.333	0.25
X''_d (pu)	0.20	0.292	0.233
X'_q (pu)	0.40	-	-
X''_q (pu)	0.20	0.292	0.225
X_l (pu)	0.15	0.15	0.15
R_s (pu)	0.01	0.01	0.01
T'_{do} (s)	7.0	5.00	6.00
T''_{do} (s)	0.05	0.002	0.002
T'_{qo} (s)	1.5	-	-
T''_{qo} (s)	0.05	0.002	0.002
H (s)	4.5	6.0	5.0

VIII. Acknowledgment

The authors gratefully acknowledge the contributions of Dr. Carlos Collados-Rodríguez respecting GFM controllers tunning and filter design.

TABLE II
GFL converters parameters.

Parameter	G4, G5, G6, G8, G9, G12
Converter-side voltage V_n (kV)	22
Transformer leakage reactance X (pu)	0.15
PLL bandwidth (rad/s)	$2\pi 80$
Current control bandwidth (rad/s)	$2\pi 135$
Power control bandwidth (rad/s)	$2\pi 13.5$
LVRT v_{max} (s)	0.9
LVRT power at v_{max} (s)	0.9
LVRT v_{min} (s)	0.5

TABLE III
GFM converters parameters.

Parameter	G2,G3	G7	G10,G14
Converter-side voltage V_n (kV)	22	22	22
Current control bandwidth (rad/s)	$2\pi 159$	$2\pi 159$	$2\pi 159$
Voltage control bandwidth (rad/s)	$2\pi 18$	$2\pi 18$	$2\pi 18$
Active power droop k_{droop} (%)	3	1	5
Filter inductance L_f (p.u)	0.2	0.2	0.2
Transformer reactance L_c (pu)	0.15	0.15	0.15
Filter resistance R_f (p.u)	0.01	0.01	0.01
Filter capacitance C (p.u)	0.15	0.15	0.15
Filter damping R_{cap} (p.u)	0.22	0.22	0.22

References

[1] P. Kundur, J. Paserba, V. Ajjarapu, G. Andersson, A. Bose, C. Canizares, N. Hatziargyriou, D. Hill, A. Stankovic, C. Taylor, T. Van Cutsem, and V. Vittal, "Definition and classification of power system stability IEEE/CIGRE joint task force on stability terms and definitions," *IEEE Transactions on Power Systems*, vol. 19, no. 3, pp. 1387–1401, aug 2004.

[2] N. Hatziargyriou, J. Milanovic, C. Rahmann, V. Ajjarapu, C. Canizares, I. Erlich, D. Hill, I. Hiskens, I. Kamwa, B. Pal, P. Pourbeik, J. S. Gasca, A. Stankovic, T. V. Cutsem, V. Vittal, and C. Vournas, "Definition and classification of power system stability – revisited & extended," *IEEE Trans. on Power Systems*, vol. 36, no. 4, pp. 3271–3281, jul 2021.

[3] V. Jalili-Marandi, V. Dinavahi, K. Strunz, J. A. Martinez, and A. Ramirez, "Interfacing techniques for transient stability and electromagnetic transient programs IEEE task force on interfacing techniques for simulation tools," *IEEE Transactions on Power Delivery*, vol. 24, no. 4, pp. 2385–2395, oct 2009.

[4] Y. Zhang, A. M. Gole, W. Wu, B. Zhang, and H. Sun, "Development and analysis of applicability of a hybrid transient simulation platform combining TSA and EMT elements," *IEEE Transactions on Power Systems*, vol. 28, no. 1, pp. 357–366, feb 2013.

[5] A. A. van der Meer, M. Gibescu, M. A. M. M. van der Meijden, W. L. Kling, and J. A. Ferreira, "Advanced hybrid transient stability and EMT simulation for VSC-HVDC systems," *IEEE Transactions on Power Delivery*, vol. 30, no. 3, pp. 1057–1066, jun 2015.

[6] S. Sanders, J. Noworolski, X. Liu, and G. Verghese, "Generalized averaging method for power conversion circuits," *IEEE Transactions on Power Electronics*, vol. 6, no. 2, pp. 251–259, apr 1991.

[7] T. Demiray and G. Andersson, "Simulation of power systems dynamics using dynamic phasor models," in *X Symposium of Specialists in Electric Operational and Expansion Planning (SEPOPE)*. , may 2006.

[8] M. Daryabak, S. Filizadeh, J. Jatskevich, A. Davoudi, M. Saeedifard, V. K. Sood, J. A. Martinez, D. Aliprantis, J. Cano, and A. Mehrizi-Sani, "Modeling of LCC-HVDC systems using dynamic phasors," *IEEE Trans. on Power Delivery*, vol. 29, no. 4, pp. 1989–1998, aug 2014.

[9] G. Love and A. Wood, "Harmonic state space model of power electronics," in *2008 13th International Conference on Harmonics and Quality of Power*. IEEE, sep 2008, pp. 1–6.

[10] M. S.-P. Hwang and A. R. Wood, "A new modelling framework for power supply networks with converter based loads and generators - the harmonic state-space," in *2012 IEEE International Conference on Power System Technology (POWERCON)*. IEEE, oct 2012.

[11] ——, "Harmonic state-space modelling of a controlled HVdc converter," *Electric Power Systems Research*, vol. 124, pp. 65–73, jul 2015.

[12] D. Shu, H. Yang, and G. He, "A harmonic phasor domain cosimulation method and new insight for harmonic analysis of large-scale VSC-MMC

based AC/DC grids," *IEEE Transactions on Power Electronics*, vol. 36, no. 4, pp. 3909–3924, apr 2021.

[13] F. Milano and A. O. Manjavacas, "Frequency-dependent model for transient stability analysis," *IEEE Transactions on Power Systems*, vol. 34, no. 1, pp. 806–809, jan 2019.

[14] G. D. Carne, M. Liserre, M. Langwasser, M. Ndreko, R. Bachmann, R. W. D. Doncker, R. Dimitrovski, B. J. Mortimer, A. Neufeld, and F. Rojas, "Which deepness class is suited for modeling power electronics?: A guide for choosing the right model for grid-integration studies," *IEEE Industrial Electronics Magazine*, vol. 13, no. 2, pp. 41–55, jun 2019.

[15] M. Paolone, T. Gaunt, X. Guillaud, M. Liserre, S. Meliopoulos, A. Monti, T. V. Cutsem, V. Vittal, and C. Vournas, "Fundamentals of power systems modelling in the presence of converter-interfaced generation," *Electric Power Systems Research*, vol. 189, p. 106811, dec 2020.

[16] CIGRE WG C4-56, *Technical Brochure 881: Electromagnetic transient simulation models for large-scale system impact studies in power systems having a high penetration of inverter-connected generation*. CIGRE, 2022.

[17] W. Lu and B.-T. Ooi, "Optimal acquisition and aggregation of offshore wind power by multiterminal voltage-source HVDC," *IEEE Transactions on Power Delivery*, vol. 18, no. 1, pp. 201–206, jan 2003.

[18] S.-K. Chung, "A phase tracking system for three phase utility interface inverters," *IEEE Transactions on Power Electronics*, vol. 15, no. 3, pp. 431–438, may 2000.

[19] H.-S. Song and K. Nam, "Dual current control scheme for PWM converter under unbalanced input voltage conditions," *IEEE Transactions on Industrial Electronics*, vol. 46, no. 5, pp. 953–959, 1999.

[20] L. Harnefors and H.-P. Nee, "Model-based current control of AC machines using the internal model control method," *IEEE Transactions on Industry Applications*, vol. 34, no. 1, pp. 133–141, 1998.

[21] C. Bajracharya, M. Molinas, J. A. Suul, and T. M. Undeland, "Understanding of tuning techniques of converter controllers for vsc-hvdc," in *Nordic Workshop on Power and Industrial Electronics (NORPIE/2008), June 9-11, 2008, Espoo, Finland*. Helsinki University of Technology, 2008.

[22] J. Svensson, M. Bongiorno, and A. Sannino, "Practical implementation of delayed signal cancellation method for phase-sequence separation," *IEEE Trans. on Power Delivery*, vol. 22, no. 1, pp. 18–26, jan 2007.

[23] M. Chandorkar, D. Divan, and R. Adapa, "Control of parallel connected inverters in standalone AC supply systems," *IEEE Transactions on Industry Applications*, vol. 29, no. 1, pp. 136–143, 1993.

[24] J. Liu, Y. Miura, and T. Ise, "Comparison of dynamic characteristics between virtual synchronous generator and droop control in inverter-based distributed generators," *IEEE Transactions on Power Electronics*, vol. 31, no. 5, pp. 3600–3611, may 2016.

[25] G.-S. Seo, M. Colombino, I. Subotic, B. Johnson, D. Gros, and F. Dorfler, "Dispatchable virtual oscillator control for decentralized inverter-dominated power systems: Analysis and experiments," in *2019 IEEE Applied Power Electronics Conference and Exposition (APEC)*. IEEE, mar 2019.

[26] C. Arghir and F. Dorfler, "The electronic realization of synchronous machines: Model matching, angle tracking, and energy shaping techniques," *IEEE Transactions on Power Electronics*, vol. 35, no. 4, pp. 4398–4410, apr 2020.

[27] Q.-C. Zhong and G. Weiss, "Synchronverters: Inverters that mimic synchronous generators," *IEEE Transactions on Industrial Electronics*, vol. 58, no. 4, pp. 1259–1267, apr 2011.

[28] J. Liu, Y. Miura, H. Bevrani, and T. Ise, "Enhanced virtual synchronous generator control for parallel inverters in microgrids," *IEEE Transactions on Smart Grid*, vol. 8, no. 5, pp. 2268–2277, sep 2017.

[29] D. B. Rathnayake, M. Akrami, C. Phurailatpam, S. P. Me, S. Hadavi, G. Jayasinghe, S. Zabihi, and B. Bahrani, "Grid forming inverter modeling, control, and applications," *IEEE Access*, vol. 9, pp. 114 781–114 807, 2021.

[30] ESIG - Energy Systems Integration group, *Grid-Forming Technology in Energy Systems Integration*, 2022. [Online]. Available: https://www.esig.energy/grid-forming-technology-in-energy-systems-integration/

[31] O. Gomis-Bellmunt, S. D. Tavakoli, V. A. Lacerda, and E. Prieto-Araujo, "Grid-forming loads: Can the loads be in charge of forming the grid in modern power systems?" *IEEE Trans. on Smart Grid*, pp. 1–1, 2022.

[32] J. Fanals-Batllori, J. Song, M. Cheah-Mañé, E. Prieto-Araujo, and O. Gomis-Bellmunt, "Grid code analysis considering converter-based grid voltage support during faults," *International Journal of Electrical Power &amp Energy Systems*, vol. 148, p. 109000, jun 2023.

[33] M. G. Taul, X. Wang, P. Davari, and F. Blaabjerg, "Current reference generation based on next-generation grid code requirements of grid-tied converters during asymmetrical faults," *IEEE Journal of Emerging and Selected Topics in Power Electronics*, vol. 8, no. 4, pp. 3784–3797, dec 2020.

[34] S. D. Tavakoli, E. Prieto-Araujo, O. Gomis-Bellmunt, and S. Galceran-Arellano, "Fault ride-through control based on voltage prioritization for grid-forming converters," *IET Renewable Power Generation*, jan 2023.

[35] V. A. Lacerda, E. P. Araujo, M. Cheah-Mane, and O. Gomis-Bellmunt, "Phasor modeling approaches and simulation guidelines of voltage-source converters in grid-integration studies," *IEEE Access*, vol. 10, pp. 51 826–51 838, 2022.

[36] E. A. Gil, M. C. Mane, C. C. Rodríguez, L. F. Llerins, J. G. Badia, O. G. Bellmunt, E. P. Araujo, E. S. Sánchez, L. Arribas, M. Biencinto, L. González, J. Polo, L. Valenzuela, Álvaro Ortega, L. Rouco, L. Sigrist, and B. Marinescu, "POSYTYF project deliverable D1.1 definition and specification of dynamic virtual power plants scenarios," 2021. [Online]. Available: https://posytyf-h2020.eu/